ACS APPLIED MATERIALS & INTERFACES

www.acsami.org

Research Article

Chemical Modification of Human Decellularized Extracellular Matrix for Incorporation into Phototunable Hybrid-Hydrogel Models of Tissue Fibrosis

Rukshika S. Hewawasam, Rachel Blomberg, Predrag Šerbedžija, and Chelsea M. Magin*

Cite This: https://doi.org/10.1021/acsami.2c18330

Read Online

ACCESS | Metrics & More | Article Recommendations | Supporting Information

ABSTRACT: Tissue fibrosis remains a serious health condition with high morbidity and mortality rates. There is a critical need to engineer model systems that better recapitulate the spatial and temporal changes in the fibrotic extracellular microenvironment and enable study of the cellular and molecular alterations that occur during pathogenesis. Here, we present a process for chemically modifying human decellularized extracellular matrix (dECM) and incorporating it into a dynamically tunable hybrid-hydrogel system containing a poly(ethylene glycol)-α methacrylate (PEGαMA) backbone. Following modification and characterization, an off-stoichiometry thiol-ene Michael addition reaction resulted in hybrid-hydrogels with mechanical properties that could be tuned to recapitulate many healthy tissue types. Next, photoinitiated, free-radical homopolymerization of excess α-methacrylates increased crosslinking density and hybrid-hydrogel elastic modulus to mimic a fibrotic microenvironment. The incorporation of dECM into the PEGαMA hydrogel decreased the elastic modulus and, relative to fully synthetic hydrogels, increased the swelling ratio, the average molecular weight between crosslinks, and the mesh size of hybrid-hydrogel networks. These changes were proportional to the amount of dECM incorporated into the network. Dynamic stiffening increased the elastic modulus and decreased the swelling ratio, average molecular weight between crosslinks, and the mesh size of hybrid-hydrogels, as expected. Stiffening also activated human fibroblasts, as measured by increases in average cellular aspect ratio (1.59 ± 0.02 to 2.98 ± 0.20) and expression of α-smooth muscle actin (αSMA). Fibroblasts expressing αSMA increased from 25.8 to 49.1% upon dynamic stiffening, demonstrating that hybrid-hydrogels containing human dECM support investigation of dynamic mechanosensing. These results improve our understanding of the biomolecular networks formed within hybrid-hydrogels: this fully human phototunable hybrid-hydrogel system will enable researchers to control and decouple the biochemical changes that occur during fibrotic pathogenesis from the resulting increases in stiffness to study the dynamic cell–matrix interactions that perpetuate fibrotic diseases.

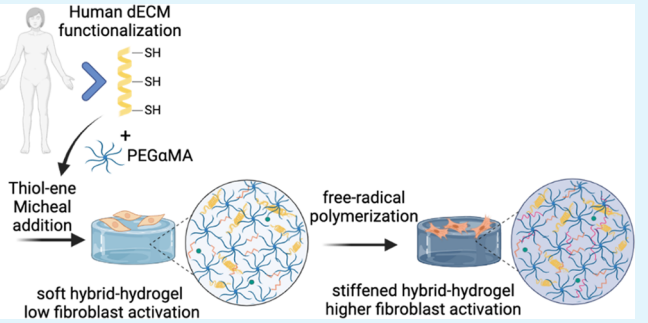

KEYWORDS: *biomaterial, hybrid-hydrogel, fibrosis, decellularized extracellular matrix, fibroblast activation*

INTRODUCTION

Progressive tissue fibrosis is a serious health condition that impacts the lungs (idiopathic pulmonary fibrosis, cystic fibrosis), liver (cirrhosis), kidney (renal fibrosis), skin (scleroderma), and other organs.[1] Fibrosis across all organ types is the result of a failed wound-healing process. Evidence suggests that an insult induces differentiation of fibroblasts into myofibroblasts, which proliferate and deposit excess extracellular matrix (ECM), resulting in fibrotic scarring and tissue stiffening.[1] This aberrant healing response initiates a positive feedback loop where fibroblasts near the injury activate in response to the stiffened microenvironment, further remodeling the ECM and spreading fibrotic tissue stiffening.[2,3] Our understanding of the initiation, progression, and potential resolution of fibrosis could be improved by engineering preclinical models that more closely replicate the dynamic nature of this disease.[4] Here, we present a process for the chemical modification of human decellularized extracellular matrix (dECM) for incorporation into hybrid-hydrogels with a phototunable poly(ethylene glycol)-α methacrylate (PEGα-MA) backbone to create biomaterial models containing relevant biochemical cues, with dynamic mechanical properties for studying fibroblast–matrix interactions *in vitro*.

Hydrogels, water-swollen polymer networks are a versatile tool for recapitulating the fibrotic microenvironment and studying specific cell–matrix interactions.[5] Naturally derived

Received: October 11, 2022
Accepted: March 7, 2023

hydrogel biomaterials, including Matrigel,[6−8] fibrin,[9,10] and collagen,[11−13] have been used extensively to study fibrosis in lung, liver, skin, and muscle. Likewise, advancements in tissue-specific decellularization have resulted in dECM hydrogels, which can model disease progression in lung,[14] liver,[15] and heart.[16] Although these biomaterials offer environments rich in endogenous biochemical cues, natural polymers that form structures through self-assembly present engineering challenges.[17] These biomaterials exhibit limited control over mechanical properties and high degradation rates that make it difficult to recapitulate the fibrotic microenvironment *in vitro*.[16,18,19] One approach to maintain ECM ligands for cellular binding and long-term culture, while enabling mechanical tunability, is chemical modification of natural materials. For example, methacrylation of gelatin and hyaluronic acid resulted in scaffolds that maintained encapsulated valvular interstitial cells (myofibroblast precursors from the heart valve leaflet) for several weeks in culture in a quiescent state.[20,21] To decouple the changes in ECM composition from subsequent mechanical changes, Nizamoglu et al. reported a strategy for tailoring the mechanical properties of human lung dECM hydrogels using ruthenium/sodium persulfate-initiated di-tyrosine crosslinking in a way that does not alter the chemical composition.[14] Similarly, Petrou et al. and Saleh et al. engineered hybrid-hydrogel systems that employed a phototunable PEGαMA backbone as a blank slate for the addition of healthy porcine lung dECM or healthy and fibrotic murine lung dECM, respectively, and showed that dynamic stiffening *in situ* increased fibroblast activation in real-time.[22,23]

Here, we build on this work by chemically modifying human dECM for incorporation into a dual-stage polymerization hybrid-hydrogel system and characterizing the resulting hydrogel networks. The dual-stage polymerization technique includes two cytocompatible steps to achieve dynamic stiffening: (1) off-stoichiometry thiol-ene Michael addition *via* step-growth polymerization and (2) homopolymerization of remaining αMA moieties *via* photopolymerization. Chemical modification of human dECM to convert primary amines to thiols enabled this naturally derived component that enhances cellular adhesion to be incorporated into the dynamic culture system. The incorporation of human dECM increased the molecular weight between crosslinks, swelling, and mesh size of the hybrid-hydrogels compared to synthetic controls, resulting in decreases in bulk elastic modulus measurements directly proportional to the amount of dECM added to the biomaterial system. The dual-stage polymerization provided controlled tunability of biomaterial mechanical properties with average elastic modulus values that matched healthy (4.8 ± 0.19 kPa) and fibrotic (13.89 ± 0.36 kPa) human tissues, pre- and post-stiffening, respectively. This dynamic increase in biomaterial modulus initiated changes in spreading and α-smooth muscle actin (αSMA) protein expression consistent with fibroblast activation. These findings enhance our understanding of the biomolecular networks formed within hybrid-hydrogels and how to employ these biomaterial systems to dynamically study the cellular and molecular mechanisms underlying fibrosis.

EXPERIMENTAL SECTION

Materials. All chemicals and reagents were purchased from commercial sources and used without further purification unless otherwise stated. Poly(ethylene glycol)-hydroxyl (PEG-OH; 8-arm, 10 kg mol^{-1}) was purchased from JenKem Technology USA, Inc. and lyophilized before use. Ethyl 2-(bromomethyl)acrylate (EBrMA) was purchased from Ambeed, Inc. Sodium hydride (NaH), 2-iminothiolane hydrochloride (Traut's reagent), and 3-(trimethoxysilyl)propyl methacrylate were purchased from Sigma-Aldrich. Human dECM (HumaMatrix) was provided by and purchased from Humabiologics, Inc.

METHODS

Poly(ethylene glycol)-α Methacrylate (PEGαMA) Synthesis. The reaction was carried out under moisture-free conditions. A flame-dried 250 mL Schlenk flask was charged with a stir bar, 10 kg mol^{-1} PEG-OH (5 g, 0.004 mol of −OH), and 80 mL of anhydrous THF (Sigma-Aldrich). Once PEG-OH was completely dissolved, NaH (0.38 g, 0.015 mol, 3.75 molar excess) was added, and the reaction mixture was stirred at room temperature for 30 min. EBrMA (3.68 mL, 0.026 mol, 6.5 molar excess) was added dropwise, and the Schlenk flask was wrapped in aluminum foil to protect the reaction from light and the mixture was stirred for 48 h at room temperature. The reaction was quenched with 1 N acetic acid and filtered through celite 545. The filtrate was concentrated under reduced pressure, and the polymer was precipitated with diethyl ether (Sigma-Aldrich) at 4 °C. The polymer was further purified using dialysis (1 kDa MWCO, Repligen) against 3.5 L of deionized water with a total of four changes over 72 h at room temperature and lyophilized to obtain a pure white solid powder. The functionalization and the purity of the product were verified by ^{1}H NMR. Only PEGαMA with functionalization over 95% by comparison of the αMA alkene end group to the PEG backbone was used in subsequent experiments.

PEGαMA Characterization. ^{1}H NMR spectrum was recorded on a Bruker DPX-400 FT NMR spectrometer (300 MHz) and, to ensure proper relaxation of the functional groups and accurate quantification, 284 scans and 2.5 s relaxation delay were modified parameters. NMR spectrum was analyzed as follows: chemical shift δ (ppm) (multiplicity, number of protons, and assignment). The chemical shifts for protons (^{1}H) were recorded in parts per million (ppm) relative to a residual solvent. PEGαMA ^{1}H NMR (300 MHz, $CDCl_3$): δ (ppm) 1.36 (t, 3H, CH_3−), 3.71 (s, 114H, PEG CH_2-CH_2), 4.29 (t, s, 4H, −CH_2−C(O)−O−O, −O−CH_2−C(=CH_2)−), 5.93 (q, 1H, −C=CH_2), 6.34 (q, 1H, −C=CH_2). Yield: 74%. End group functionalization of the final PEGαMA polymer was greater than 99% by comparison of the αMA alkene end group to the PEG backbone (Figure S1).

Human dECM Functionalization. Free primary amines on human dECM (HumaMatrix, Humabiologics, Inc.) were converted to thiols to create a clickable dECM crosslinker compatible with a thiol-ene Michael addition reaction. Primary amine concentration was quantified using a standard ninhydrin assay (Sigma-Aldrich) performed according to the manufacturer's protocol. Traut's reagent in PBS (pH 7.4) was reacted with the free amines that naturally occur on human dECM proteins in 3 mM ethylenediaminetetraacetic acid (EDTA, Thermo Fisher) for 1 h at room temperature. The molar excess of Traut's reagent required to minimize amine content following thiolation was identified by measuring amine content after dECM reaction with 5, 10, 25, 50, 75, and 100 molar excess of Traut's reagent. Thiolated dECM was purified by dialysis (100−500 Da MWCO, Repligen) against deionized water at room temperature and lyophilized to obtain a solid powder. Free thiol content was quantified using Ellman's reagent (5,5′-dithiobis(2-nitrobenzoic acid), Sigma-Aldrich) according to the manufacturer's protocol. Absorbance was measured using BioTek Synergy H1: modular multimode microplate reader, with monochromator-based optics and filter-based optics.

Human dECM Characterization. Free primary amine content and free thiol content were quantified pre- and post-thiolation treatment. The concentration of protein within each dECM solution pre- and post-thiolation treatment was measured by absorbance (λ = 260/280) using BioTek Synergy H1: modular multimode microplate reader using a Take3 Micro-Volume Plate (Figure S2). The protein molecular weight distribution of dECM fragments before and after

https://doi.org/10.1021/acsami.2c18330
ACS Appl. Mater. Interfaces XXXX, XXX, XXX−XXX

thiolation was measured by loading equal concentrations of protein based on absorbance measurements of concentration and then separating the proteins using sodium dodecyl sulfate−polyacrylamide gel electrophoresis (SDS-PAGE). Briefly, electrophoresis was performed on 4−20% Mini-PROTEAN TGX Precast Protein Gels for approximately 120 min at 100 V in a tris borate buffer, per the manufacturer's protocol. A QuickStain Protein Labeling Kit (Amersham) stained bands for fluorescent imaging and qualitative evaluation.

Hybrid-Hydrogel Fabrication. Synthesized PEGαMA was reacted with thiolated human dECM and DTT (Sigma-Aldrich) crosslinkers off-stoichiometry (3:8 thiol to αMA) in a base-catalyzed Michael addition reaction. The weight percent (wt %) of the PEGαMA polymer backbone and the ratio between dECM and DTT crosslinkers were varied to achieve the desired elastic modulus values before and after a secondary crosslinking reaction. TCEP (tris(2-carboxyethyl)phosphine Sigma-Aldrich) was used as a reducing agent to maximize the free thiol content in human dECM. The TCEP molar excess required for maximum free thiol concentration was determined using an Ellman's assay (Figure S3). Prior to hybrid-hydrogel fabrication, thiolated human dECM (0.012 mg μL^{-1}) was dissolved in 250 mM TCEP and incubated for 1 h at a 20 molar excess to the thiol concentration as determined by Ellman's assay. Stock solutions of PEGαMA (0.4 mg μL^{-1}), DTT (Sigma-Aldrich) (250 mM), and CGRGDS (GL Biochem); a peptide sequence that mimics the cell-adhesive ligands on fibronectin (75 mM) were prepared in 0.3 M, pH 8 HEPES ((4-(2-hydroxyethyl)-1-piperazineethanesulfonic acid), Sigma-Aldrich) solution. Both crosslinkers and CGRGDS were combined and added to the PEGaMA to make the precursor solution. Drops (40 μL) of precursor solution were placed between two hydrophobic glass slides covered with parafilm and kept for 30 min at 37 °C to polymerize. Polymerized hydrogels were equilibrated in PBS at room temperature with or without 2.2 mM lithium phenyl-2,4,6-trimethyl-benzoylphosphinate photoinitiator (LAP; 0.06 wt %; Sigma-Aldrich) overnight. Hydrogels equilibrated with LAP photoinitiator were exposed to UV light (365 nm,10 mW cm^{-2}) for 5 min using an OmniCure Series 2000 UV lamp to obtain stiffened hybrid-hydrogels *via* homopolymerization of free excess αMA moieties.

Hybrid-Hydrogel Characterization. *Rheological Measurement of Hydrogel Mechanical Properties.* Rheological analysis was performed using a Discovery HR2 rheometer (TA Instruments) with an 8 mm parallel plate geometry and the Peltier plate set at 37 °C. Hybrid-hydrogels were analyzed after each polymerization reaction. The geometry was lowered until the instrument read 0.03 N axial force and the gap distance was noted. The gap distance between the plate and the geometry was adjusted until the storage modulus measurement (G') plateaued and a percent compression of the specific hydrogel was defined and used thereafter. Samples were subjected to frequency oscillatory strain between 0.1 and 100 rad s^{-1} at 1%. The elastic modulus (E) was calculated using rubber elastic theory and G' measurements, which were converted assuming a Poisson's ratio of 0.5 for bulk measurements of elastic hydrogel polymer networks.[24] To assess whether elastic moduli between soft and stiffened gels were significantly different, a one-way ANOVA with Tukey's multiple comparison correction was performed.

Measurement of Hydrogel Swelling Ratio. Hydrogels were synthesized as described above. Soft and stiffened synthetic and hybrid-hydrogels ($n = 6$) were swollen in deionized water for 48 h to allow hydrogels to swell to equilibrium. Unsubmerged mass (m) and submerged mass (m') of the just-synthesized hydrogels and swollen hydrogels were measured using the density kit to obtain Buoyancy-based volumetric measurements: V_r (relaxed volume) and V_s (swollen volume), respectively. Hexane (density (ρ) = 0.659 g mL^{-1}) was used as the nonsolvent solution for the density kit. V_r and V_s were calculated using eq 1.[25]

$$V_{r/s} = \frac{m - m'}{\rho} \tag{1}$$

Hydrogels were freeze-dried to remove all solvent and the dried polymer was weighed using the Mettler Toledo MS104TS balance. The dried volume (V_d) of the polymer was calculated using the PEG polymer density as 1.12 g cm^{-3} and the weight of the dried polymer. The volumetric swelling ratio (Q) was calculated using eq 2.[25]

$$Q = \frac{V_s}{V_d} \tag{2}$$

Equilibrium Swelling Theory Calculations. Mesh size (ξ) is the average distance between two neighboring network junctions connected by a polymer chain in a hydrogel. To estimate mesh size, the average molecular weight between crosslinks in a polymer network (M_c) was calculated using the Flory−Rehner eq 3, which compares the entropic contribution of mixing polymer and solvent with the elastic energy created as the polymer network swells to incorporate solvent.[26]

$$\frac{1}{M^c} = \frac{2}{M^n} - \frac{1/\rho^d V^l[\ln(1-\varphi^s) + \varphi^s + \chi\varphi^{s2}]}{\varphi^r\left[\left(\frac{\varphi^s}{\varphi^r}\right)^{1/3} - \frac{1}{2}\left(\frac{\varphi^s}{\varphi^r}\right)\right]} \tag{3}$$

where M_n is the number-average molecular weight of an uncrosslinked polymer (10,897 g mol^{-1}), V_l is the molar volume of water (18 mL mol^{-1}), and χ is the polymer−solvent interaction parameter (taken to be 0.426 for PEG in water).[27] φ_s is the swollen polymer volume fraction, calculated as V_d/V_s, and φ_r is the polymer volume fraction in the relaxed state, calculated as V_d/V_r. The mesh size was subsequently obtained using the universal version of the Canal−Peppas equation (eq 4).[26]

$$\xi = \varphi^{s^{-1/3}}\left[\left(1 - \frac{2}{f}\right)\bar{r}^2 C\infty \frac{\lambda M_c}{M_r}\right]^{1/2} \tag{4}$$

The characteristic ratio (C_∞) is independent of the length of the chain in a phantom network model and it was taken as 4 for PEG polymers.[25] The weighted average of polymeric backbone bond length per repeating unit ($\bar{r}$) was considered as 0.146 nm.[28] The molecular weight of the polymer repeating unit (M_r) was used as 44 g mol^{-1}. The number of backbone bonds in the polymer repeating unit (λ) is 3 for PEG polymers. The branching factor of the macromonomers (f) was taken as 8, assuming 100% functionalization with methacrylate groups, respectively, and 100% reaction during crosslinking.

Estimation of Theoretical Shear Modulus. Shear modulus (G) was calculated according to the Rubberlike elasticity theory using eq 5.[25] G is the polymer network's shear modulus, R is the ideal gas constant, and T is the absolute temperature of the system. The frequency of chain-end defects (γ) is considered as 0.5, which would mean that only half of the network chains are connected to two junctions in each condition.

$$G = RT\left[\left(1 - \frac{2}{f}\right)(1-\gamma)\frac{\rho^d}{M_c}\varphi^{r^{2/3}}\varphi^{s^{1/3}}\right] \tag{5}$$

It is important to note that while these equations were originally developed for synthetic materials, and have been used to evaluate hybrid-hydrogel materials by several research groups,[29,30] there may be differences between the behavior of fully synthetic hydrogel networks and those containing biological molecules.

ECM Component Staining. Hybrid-hydrogels were equilibrated overnight in PBS before being processed for cryosectioning and either Picrosirius red (Abcam) staining for collagen or Alcian blue (Sigma) staining for glycosaminoglycans. Hydrogels were submerged in optimal cutting temperature (OCT) compound (Sakura) for 48 h at room temperature in a humidified chamber to allow for complete infusion of the compound. Three infused hydrogel samples per condition were stacked in a 15 mm × 15 mm × 5 mm vinyl cryomold (Sakura) and flash-frozen by submersion in liquid nitrogen-cooled 2-methylbutane (Sigma-Aldrich). Frozen samples were removed from the mold and mounted lengthwise onto a Leica CM1850 cryostat such that each cut would take a cross section of the hydrogel stack. 10

https://doi.org/10.1021/acsami.2c18330
ACS Appl. Mater. Interfaces XXXX, XXX, XXX−XXX

μm sections were acquired from regions throughout the hydrogel stack.

For collagen staining, frozen slides were equilibrated to room temperature in deionized water (5−10 min). Then, slides were submerged in Picrosiruis red solution for 1 h. Slides were then briefly dipped into two changes of fresh 0.5% acetic acid to clear any unbound dye. Slides were dehydrated by sequential submersion in 100% ethanol (2 min × 5 min) and SafeClear II (2 min × 5 min, Fisher Scientific) before being mounted in Cytoseal 60 (Thermo Fisher) under a 24 mm × 50 mm coverslip (Globe Scientific). Imaging was performed on a brightfield microscope (Olympus CKX53 microscope, EP50 camera). To quantify the distribution of collagen within these cross sections, densitometry analysis was performed in Fiji (ImageJ) by converting the color image to grayscale, drawing a region of interest around the stained section, and generating a histogram of relative stain intensity across the length of the hydrogel cross section.

For glycosaminoglycan staining, frozen slides were brought to room temperature and equilibrated in deionized water (5−10 min). Slides were then submerged in Alcian blue solution (1% Alcian blue 8GX in 3% acetic acid, final pH 2.5) for 30 min. Slides were then rinsed under running tap water for 5 min, washed by submersion in deionized water for 3 min, and then dehydrated and imaged as above.

Fibroblast Culture. Human pulmonary fibroblasts (ATCC cat. # CCL-151) were passaged at least twice prior to use and incubated in a complete medium consisting of Dulbecco's Modified Eagle Medium/F-12 (DMEM/F-12) containing 10% fetal bovine serum (FBS, Thermo Fisher), 100 U mL^{-1} penicillin, 100 U mL^{-1} streptomycin, and 0.5 μg mL^{-1} amphotericin (Life Sciences) at 37 °C and 5% CO_2. The culture medium was changed every 2−3 days, and the cells were grown to approximately 80% confluency before passaging or seeding onto hybrid-hydrogels between passages two and seven.

Fibroblast Activation Experiments. Fibroblast activation experiments were conducted under aseptic conditions. Hybrid-hydrogels were fabricated using 15 wt % PEGαMA and a 90:10 DTT/dECM crosslinker ratio as described above. All hydrogel components were dissolved in sterile pH 8 HEPES. Cell culture samples were prepared by silanating 18 mm glass coverslips (Fisher Scientific) with 3-(trimethoxysilyl)propyl methacrylate using a liquid deposition technique.[31] 90 μL droplets of hybrid-hydrogel precursor solution were placed between each silanted coverslip and a hydrophobic glass slide treated with SigmaCote (Sigma-Aldrich) according to manufacturer instructions. Hybrid-hydrogels were allowed to polymerize for 30 min at 37 °C and were equilibrated in sterile PBS for 3 h at room temperature. PBS was replaced with complete medium, and hydrogels were incubated at 37 °C overnight prior to experiments. Fibroblasts were seeded onto hybrid-hydrogels at a density of 20,000 cells/cm^2 for immunocytochemistry and incubated at 37 °C and 5% CO_2 overnight. The following day (Day 1), the serum content of the culture medium was reduced to 1%. The medium was changed on Day 3 and Day 5. On Day 7, cells on soft hydrogels were processed for immunocytochemistry as described below. To obtain stiffened hybrid-hydrogels, the cell culture medium was supplemented with a 2.2 mM LAP photoinitiator on Day 6 and hydrogels were exposed to UV light (365 nm, 10 mW cm^{-2}) for 5 min using an OmniCure Series 2000 UV lamp (Lumen Dynamics). LAP was removed after a 45 min incubation at 37 °C and the cell culture medium was replaced to allow for additional incubation at 37 °C and 5% CO_2 for two more days. On Day 9, cells on stiffened hydrogels were processed for immunocytochemistry.

Immunostaining. Unless otherwise specified, all steps were performed at room temperature. Cells were fixed and permeabilized with 0.5 wt % Triton X-100 (0.1%; Fisher BioReagents) in 4% v/v paraformaldehyde in PBS for 10 min. Excess paraformaldehyde was quenched with 100 mM glycine (Sigma-Aldrich) in PBS for 15 min, and cells were rinsed with PBS. Nonspecific binding sites were blocked with 5% bovine serum albumin (BSA, Sigma-Aldrich) in PBS for 1 h. Mouse anti-human α-smooth muscle actin (αSMA) monoclonal antibody (Thermo Fisher Scientific; clone 1A4) was diluted 1:250 in 3% BSA/0.1% tween-20 (Fisher Scientific) and incubated for 1 h. Samples were rinsed three times with PBS and incubated in 1:250 goat anti-mouse AlexaFluor555 (Thermo Fisher Scientific) secondary antibody in 3% BSA/0.1% tween-20 supplemented with Actin 488 Ready Probes (Thermo Fisher Scientific) for 1 h. Nuclei were counter-stained with 0.5 μg mL^{-1} DAPI in PBS for 10 min and samples were rinsed three times with deionized water. Cell-seeded hydrogels were mounted onto microscopy slides face up and preserved for imaging with Prolong Gold Antifade (Life Sciences) under a 22 mm coverslip. All microscopy was performed on a BX-63 upright epifluorescent microscope (Olympus). Five fields of view were randomly selected on each hydrogel and imaged with a 10× objective.

Image Analysis. Image analysis was performed with Fiji (ImageJ) software (NIH). Cell nuclei (DAPI channel for immunofluorescent stains or both total and dead dyes for live/dead analysis) were counted by establishing a signal threshold, performing a watershed operation, and analyzing particles. Activated fibroblasts were counted on the αSMA channel by establishing a signal threshold above background and analyzing for particles with a circularity less than 0.5, indicating increased spreading, a characteristic of activation fibroblasts.[32]

$$\text{circularity} = 4\pi\left(\frac{\text{area}}{\text{perimeter}^2}\right)$$

To calculate the percentage of activated cells per sample, this count was divided by the total number of cell nuclei. Cell spreading was quantified on the f-actin channel by establishing a signal threshold and analyzing particles using the fit ellipse function. The aspect ratio was calculated by taking the ratio of the major axis to the minor axis of each ellipse generated by this function. All fibroblast activation experiments were performed using at least $n = 3$ technical replicates, where each replicate was an individual hydrogel sample in a separate well. The experiments were repeated three times starting on separate days with different flasks of fibroblasts from the same source. Five representative fields of view at least 2 mm from the edge of the hydrogel surface were systematically imaged and analyzed for each sample.

RESULTS AND DISCUSSION

Chemical Modification of Human Decellularized Extracellular Matrix. During fibrotic progression, the biochemical composition, organization, and biomechanics of the ECM change dramatically.[33] Increased ECM synthesis and remodeling leads to changes in the expression of core matrisome and matrisome-associated proteins and proteoglycans. Excessive accumulation of fibrillar collagen occurs due to an imbalance in collagen synthesis and assembly relative to degradation, which results in tissue stiffening in nearly every major organ.[34] Healthy liver is typically soft (<6 kPa) with low amounts of fibrillar collagens, such as collagen I.[35] Collagen mass was shown to increase 7-fold in severely fibrotic livers according to hydroxyproline analysis[36] and histology.[37] Subsequently, liver stiffness increased to pathologic levels (>20 kPa); this increase in stiffness was correlated with increased portal pressure, an indicator of cirrhosis.[35] Analyses of fibrotic human heart tissues revealed increases in collagens I and IV, laminin-γ1, fibrillin-1, and periostin. Normal heart tissue has an elastic modulus of 10−15 kPa, while fibrotic tissue can be anywhere from 2 to 10 times stiffer.[38] Excessively stiff heart tissue impacts distensibility, impedes pumping, and contributes to diastolic and systolic dysfunction.[38] Healthy lung tissue is relatively soft, ranging from 1 to 5 kPa, and can stiffen above 10 kPa in pulmonary fibrosis.[39] These large changes in elastic modulus across various organs are all at least partially attributable to increases in fibrillar collagens, which are also accompanied by higher levels of other ECM proteins,

https://doi.org/10.1021/acsami.2c18330
ACS Appl. Mater. Interfaces XXXX, XXX, XXX−XXX

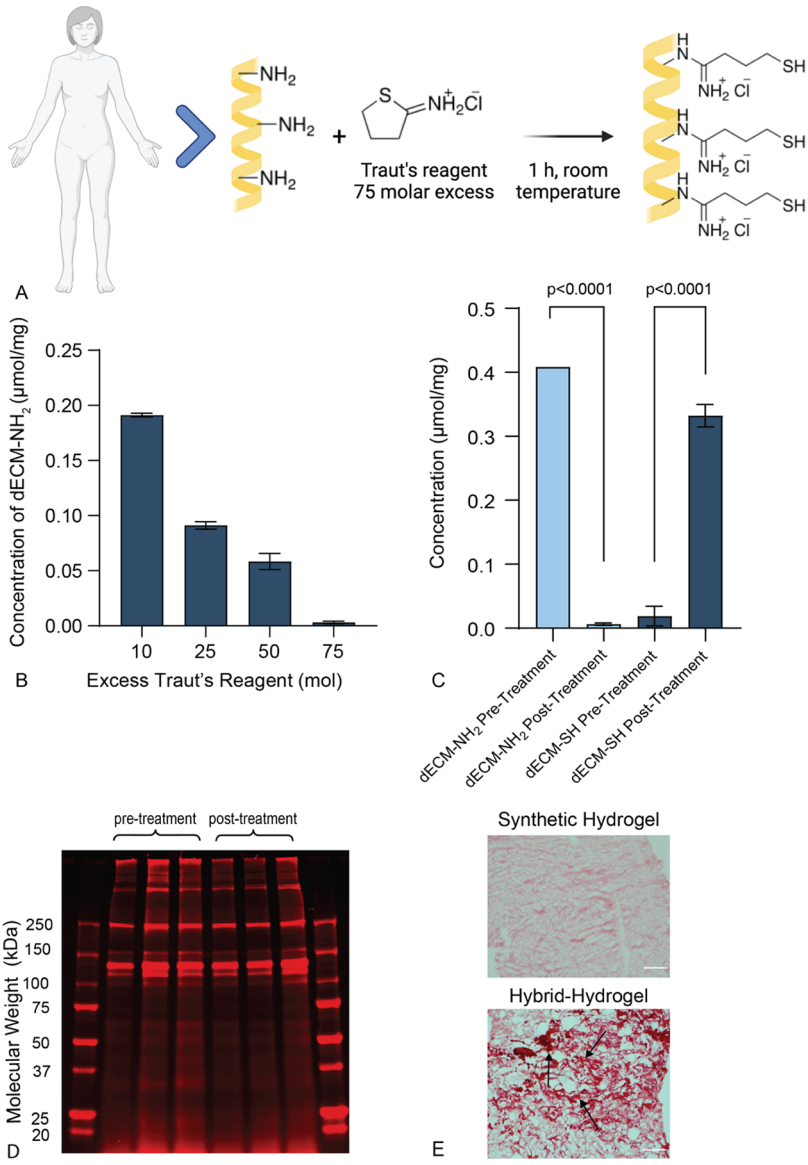

Figure 1. (A) Chemical reaction scheme for human dECM thiolation with Traut's reagent. Figure created with BioRender.com. (B) Selection of minimum Traut's reagent molar excess required to convert primary amines to thiols on human dECM. The minimum concentration of primary amine was obtained at 75 molar excess of Traut's reagent (n = 3, ANOVA). (C) Variation of primary amine and thiol concentration measured in human dECM pre- and post-thiolation process *via* ninhydrin and Ellman's assays, respectively (n = 3, paired t-test). Statistically significant decreases in primary amine concentration and corresponding increases in thiol concentrations demonstrated successful chemical modification of human dECM. (D) SDS-PAGE results verified there was no significant degradation of the protein from the thiolation process. Prominent bands at 250 and 130 kDa showed large protein fragments from human dECM remained intact (n = 3). (E) Representative images of sections from the center of synthetic and hybrid-hydrogels stained with Picrosirius red to visual dECM distribution. Synthetic hydrogels consisted of 100% DTT crosslinker and hybrid-hydrogels contained crosslinkers that were 10% human dECM and 90% DTT. Black arrows point to collagen strands (dark red) distributed throughout the hybrid-hydrogels.

including tenascin-C, fibrillin-1, laminins, and vitronectin.[34] In fact, density measurements of decellularized lung tissues, which contain a high proportion of collagens, revealed that fibrotic ECM was more than twice as dense as ECM from nonfibrotic controls.[40,41] Since excessive accumulation of collagen-rich ECM with altered biochemical composition is a hallmark of fibrosis and results in increased tissue stiffness, it is crucial for *in vitro* models of fibrosis to both incorporate and decouple the biochemical and dynamic biophysical characteristics of fibrotic ECM to enable research on each contribution.

Here, we recapitulate healthy and fibrotic extracellular microenvironments by chemical functionalization and incorporation of intact human dECM into dynamically tunable PEG-based hybrid-hydrogels. Naturally occurring free primary amines on the human dECM were thiolated using Traut's reagent (Figure 1A). The average primary amine concentration of untreated human dECM was 0.41 ± 0.02 μmol mg^{-1} as measured by a ninhydrin assay. Previous studies by our group have measured the primary amine concentration for untreated porcine lung dECM (0.18 ± 0.01 μmol mg^{-1}), healthy murine lung dECM (0.40 ± 0.03 μmol mg^{-1}), and fibrotic murine lung dECM (0.27 ± 0.01 μmol mg^{-1}).[22,23] These small differences in primary amine concentration by species and disease state can influence the final functionality of the dECM

https://doi.org/10.1021/acsami.2c18330
ACS Appl. Mater. Interfaces XXXX, XXX, XXX−XXX

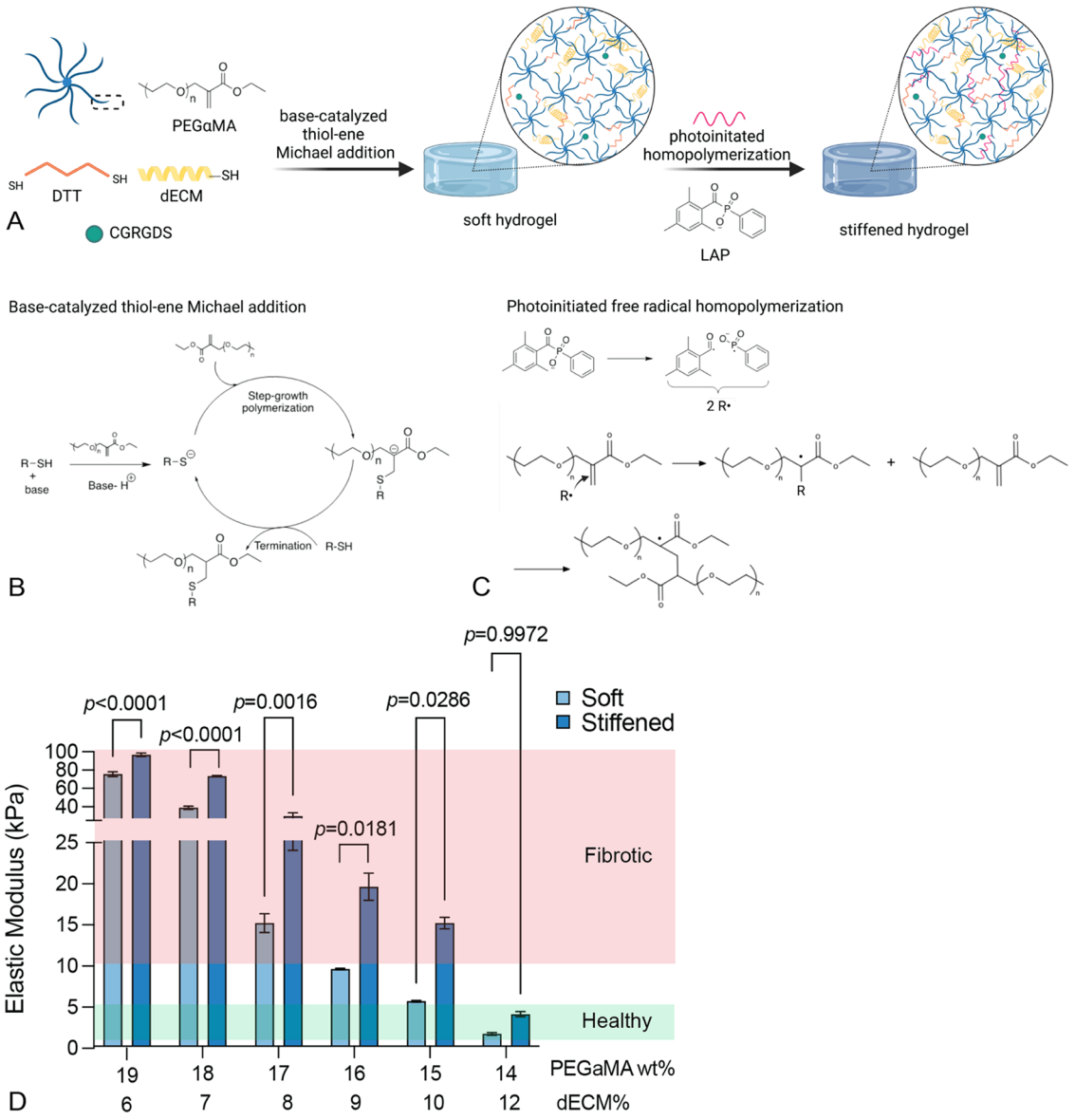

Figure 2. (A) Schematic of the dual-stage polymerization reaction that combined PEGαMA and the chemically modified human dECM crosslinker with DTT and CGRGDS to enable spatiotemporal control over stiffening. (B) Thiol-ene Michael reactions are base-catalyzed reactions where the proton abstraction by the base generates a thiolate anion and a conjugate acid. The potent nucleophile thiolate anion attacks the electrophilic β-carbon of the acrylate, forming the intermediate carbon-centered anion. This anion picks the proton from the conjugate acid and regenerates the base. Subsequently, the anionic propagation undergoes in a stepwise manner. (C) Excess αMA groups in soft hydrogels were subjected to free-radical homopolymerization using LAP as the photoinitiator. UV radiation cleaves LAP homolytically, producing two radicals. Initiator radicals attack the αMA and form a sigma bond between polymer chains increasing the crosslink density and stiffening the hydrogel. (D) Elastic modulus of soft and stiffened hybrid-hydrogels decreased with increasing dECM content ranging from 12 to 6 mol % dECM and with reducing PEGαMA wt % from 19 to 14% (n = 3, paired t-test). Figure created with BioRender.com.

crosslinker and have been accounted for in subsequent hybrid-hydrogel formulations. To identify the best concentration of Traut's reagent for conversion of primary amines to thiols, increasing molar ratios of Traut's reagent were reacted with human dECM and the final primary amine concentration was measured by ninhydrin assay. Primary amine concentration decreased as Traut's reagent molar excess in the thiolation process increased, plateauing at 75 molar excess (Figure 1B). Using a 75 molar excess of Traut's reagent, the primary amine concentration of human dECM significantly decreased from 0.41 ± 0.02 to 0.0063 ± 0.001 μmol mg^{-1}, showing that Traut's reagent reacted with the primary amines to introduce thiol functional groups on intact human dECM. The average free thiol concentration was measured using Ellman's assay pre-and post-thiolation process. Free thiol concentration was increased significantly from 0.019 ± 0.03 to 0.33 ± 0.03 μmol mg^{-1}, achieving 94% conversion of primary amines to free thiols (n = 6, p < 0.0001, ANOVA) (Figure 1C). Previous studies that performed similar chemical functionalization of dECM showed that the free thiol concentration in porcine lung dECM was approximately 0.2 μmol mg^{-1} after thiolation and that pepsin-digested healthy murine lung dECM was 0.3 μmol mg^{-1}, aligning with the human dECM thiol concentrations achieved through the process in this study.[22,23]

The structural proteins, matrix-associated growth factors, and proteoglycans in human dECM are powerful modulators

https://doi.org/10.1021/acsami.2c18330
ACS Appl. Mater. Interfaces XXXX, XXX, XXX−XXX

of cellular organization and function. Several assays were performed to verify that the thiolation process did not significantly alter these essential components that comprise human dECM. First, protein molecular weight distribution was analyzed pre- and post-thiolation. Proteins from pre- and post-treatment human dECM were separated by molecular weight using sodium dodecyl sulfate−polyacrylamide gel electrophoresis (SDS-PAGE). Next, total protein was visualized using a Cy5 NHS ester dye. This analysis showed that high-molecular-weight proteins remained even after the thiolation process, with prominent bands at 250 and 130 kDa, indicating that large protein fragments were not degraded during chemical functionalization and were available for incorporation into hybrid-hydrogels (Figure 1D). Similarly, Burgess et al., showed that protein contents detected by SDS-PAGE in native human lung tissue, decellularized lung, and pepsin-digested lung dECM were consistent, indicating that chemical digestion and mechanical digestion did not degrade the protein content.[42] This study also assessed dECM using SDS-PAGE and noted prominent bands at 130 kDa and above 250 kDa, in agreement with the results presented here. Matrix-bound growth factors are another critical component of the ECM. Pre- and post-thiolation dECM was analyzed using a human growth factor array to determine whether growth factors and the associated receptors present in the dECM were preserved through the thiolation process. A broad range of growth factors, including members of the fibroblast growth factor (FGF), platelet-derived growth factor (PDGF), and transforming growth factor-β (TGF-β) families, were detected before and after thiolation. Epidermal growth factor receptor (EGFR) was the only factor reduced post-thiolation (Figure S4). Hybrid-hydrogels were stained with Alcian blue to visual glycosaminoglycans (GAGs). Lack of positive staining showed there were no GAGs remaining after decellularization and functionalization (Figure S5), which is consistent with prior published results suggesting that traditional detergent-based decellularization processes result in the depletion of GAGs from dECM.[43] A Picrosirius red stain was applied to cross sections of both fully synthetic and hybrid-hydrogels to confirm that large collagen fragments were successfully incorporated into these biomaterials.[44] Fully synthetic hydrogels served as negative controls and showed no collagen incorporation by staining light pink with no dark red clusters, while hybrid-hydrogels showed distributed collagen fibrils (bright red) (Figure 1E) throughout the samples. Some hybrid-hydrogels showed an accumulation of these fibrils more toward the center of the hydrogel sample (Figure S6), and therefore in subsequent studies of cell behavior, analysis focused on cells away from the edges of the hydrogel. It is important to note that fibrillar collagen is not the only component of dECM, and therefore no conclusions about the distribution of all dECM components can be made by observing these images. In a previous study conducted by our group, scanning electron microscopy revealed that fibrillar protein structures were present after dECM incorporation into hybrid-hydrogels.[22]

Hybrid-Hydrogel Fabrication and Characterization. Following chemical modification, thiolated dECM was incorporated into hybrid-hydrogels featuring a dual-stage polymerization mechanism. Hybrid-hydrogels were composed of PEGαMA crosslinked with thiolated human dECM and DTT. PEGαMA was selected as the polymer backbone due to its hydrolytic stability over traditional PEGMA. The unique position of the PEGαMA ester bond allows hydrolysis to occur without affecting the hydrogel network. The αmethacrylate moiety also provides higher reactivity during chain growth polymerization.[22] Hydrolytic stability of stiffened PEGαMA hybrid-hydrogels was compared to stiffened synthetic PEGMA hydrogels by Petrou et al. and showed that PEGαMa hydrogel modulus values were stable over 60 days under cell culture conditions while PEGMA synthetic hydrogels started to degrade after only 10 days.[22]

To form soft hybrid-hydrogels, first, a base-catalyzed thiol-ene Michael addition reaction was carried out off-stoichiometry with a 3:8 ratio between free thiols and α-methacrylate functional groups. Thermodynamically favorable C−S bonds were formed between the α-methacrylate and thiol groups *via* step-growth polymerization, resulting in soft hybrid-hydrogels (Figure 2A1). Next, excess α-methacrylate groups were subjected to free-radical homopolymerization to achieve dynamic stiffening, increasing the elastic moduli of hybrid-hydrogel samples (Figure 2A2). Both the molar ratio of thiolated human dECM to DTT crosslinkers and the weight percent of PEGαMA were varied to obtain a hydrogel formulation that could exhibit a dynamic stiffening that recapitulates the transition from healthy to fibrotic human tissue.

Rheological studies were carried out to quantify the shear modulus (G) of hybrid-hydrogels containing varying ratios of human dECM/DTT and PEGαMA weight percents. G was converted to elastic modulus E assuming a fully elastic polymer network using a Poisson's ratio of 0.5 according to the rubber elasticity theory.[45] For both soft and stiffened hydrogels, elastic moduli decreased with increasing dECM content and decreasing PEGαMA weight percent as expected and as previously demonstrated in other studies.[23] Soft hybrid-hydrogels ranged from 1.51 ± 0.16 kPa up to 73.41 ± 2.56 kPa and could stiffen from 3.93 ± 0.32 to 94.42 ± 1.98 kPa (Figure 2B). These ranges encompassed the soft and stiffened elastic modulus values of several healthy and fibrotic human tissues. For instance, healthy human liver has a reported elastic modulus of <6 kPa, which can increase to over 20 kPa during fibrotic disease progression.[35] Healthy human kidney tissues have a healthy modulus of 7.76 ± 5.16 kPa, while fibrotic tissues were measured to be 12.83 ± 9.80 kPa.[46] Several studies have shown that human healthy lung tissue has an elastic modulus ranging between 1.65 ± 0.2 and 5.6 ± 1.4 kPa, whereas fibrotic human lung tissues have been measured to range from 5.3 ± 1.1 to 16.52 ± 2.25 kPa.[34] Here, chemically modified human dECM was successfully incorporated into a hybrid-hydrogel system that facilitates spatiotemporal control over precise increases in elastic modulus to recapitulate dynamic increases in human tissue stiffness that occur during fibrotic disease progression.

dECM alone can form hydrogels by self-assembly with concentration-dependent mechanical properties.[47] Pouliot, et al showed that the shear modulus of human lung dECM hydrogels could range from G = 15 to 60 Pa, which was significantly softer than healthy lung tissue.[47] While naturally derived hydrogels allow for the study of cell−matrix interactions, these systems are not ideal for studying mechanosensing due to the relatively soft, static modulus values achievable with self-assembly. Similarly, using lung dECM, de Hilster et. al. demonstrated that dECM hydrogels formed from fibrotic dECM were stiffer than those formed from healthy dECM; however, these hydrogels were

https://doi.org/10.1021/acsami.2c18330
ACS Appl. Mater. Interfaces XXXX, XXX, XXX−XXX

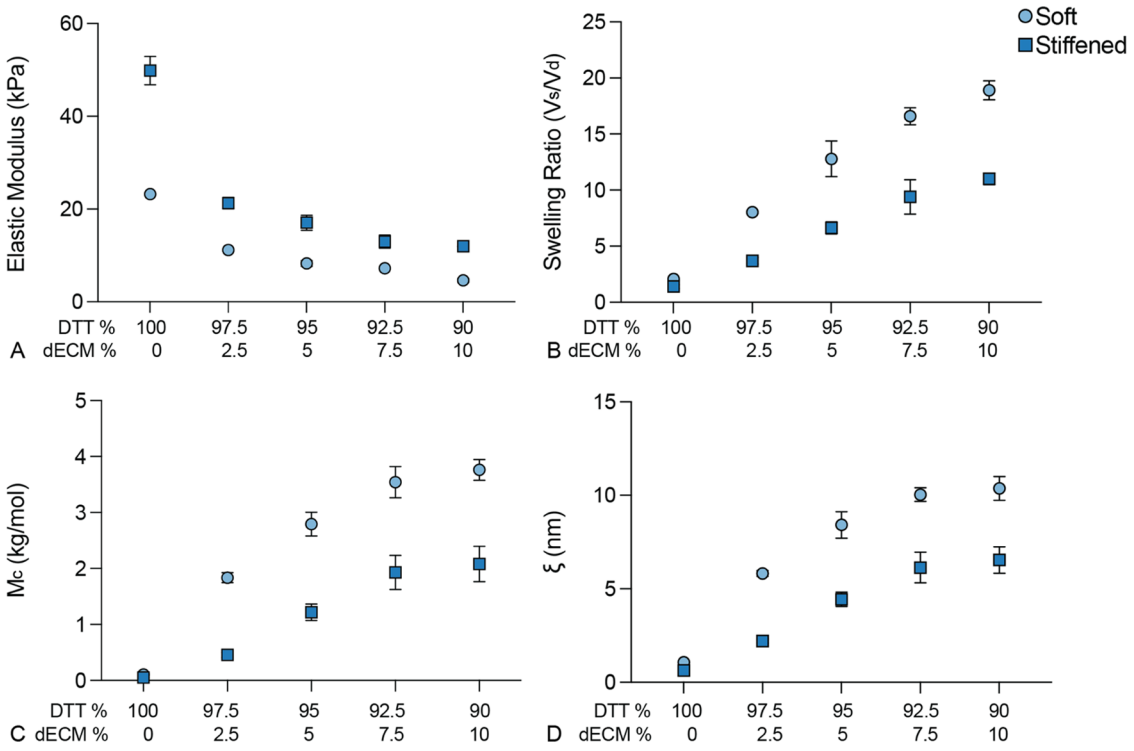

Figure 3. Mechanical properties of hybrid-hydrogels at different human dECM mol %. (A) Elastic moduli of soft and stiffened hybrid-hydrogels decreased with increasing dECM content ranging from 0 to 10 mol % dECM (n = 6, error bars, SEM). (B) Volumetric swelling ratio, (C) number-average molecular weight between crosslinks in a polymer network (M_c), and (D) mesh size of the network, respectively, increased with increasing dECM content ranging from 0 to 10 mol % dECM (n = 6, SEM). 100% DTT with 0% dECM; synthetic hydrogel has lower swelling, M_c, and mesh size compared to the hybrid-hydrogels.

significantly softer than the tissues the dECM was originally derived from, and thus failed to fully recapitulate the physiological microenvironment.[19] To overcome this limitation, photo-crosslinkable methacrylated porcine liver ECM was used to design hydrogels that could achieve stiffnesses as high as 162 kPa, demonstrating the utility of chemically modifying dECM to achieve better control over mechanical properites.[15]

In this report, human dECM was chemically modified for incorporation into hybrid-hydrogels to enable dynamic control over mechanical properties and recapitulate the mechanical properties of healthy and fibrotic human lung tissues. This hybrid-hydrogel system then modeled human pulmonary fibrosis, specifically, the activation of human lung fibroblasts in response to increasing microenvironmental stiffness. Therefore, it is important to note that hybrid-hydrogels formulated with 15 wt % PEGαMA and 10:90 dECM/DTT along with 2 mM CGRGDS exhibited an initial elastic modulus of 4.8 ± 0.19 kPa, recreated the modulus of healthy human lung tissue (1−5 kPa),[2] and were selected as the starting material for subsequent experiments. The elastic modulus for the stiffened hybrid-hydrogels, obtained after a photoinitiated, free-radical homopolymerization, was 13.89 ± 0.36 kPa, which matched levels of fibrotic lung stiffness (>10 kPa) (Figure 2B).[2,34] This dynamic tunability enabled studies of fibroblast activation in response to increased microenvironmental stiffness within a fully human model of pulmonary fibrosis.

The influence of dECM content on hybrid-hydrogel network formation and subsequent mechanical properties was analyzed and compared to fully synthetic PEGαMA controls. The elastic moduli and swelling ratios for both synthetic and hybrid-hydrogels were measured and used to calculate the average molecular weight between crosslinks, mesh size, and theoretical storage modulus (G') based on equilibrium swelling theory. The synthetic hydrogel was synthesized using 15 wt % PEGαMA along with 100% DTT. Hybrid-hydrogels were synthesized using 15 wt % PEGαMA with varying ratios of dECM/DTT (2.5, 5, 7.5, and 10%), i.e., increasing amounts of dECM crosslinker. The elastic modulus was directly related to the amount of human dECM present in hybrid-hydrogel. As dECM content increased, the elastic modulus of hybrid-hydrogel samples decreased (Figure 3A). The elastic modulus of soft fully synthetic hydrogels was 23.22 ± 0.25 kPa, while the elastic modulus of soft hybrid-hydrogels containing 10% human dECM was 4.62 ± 0.41 kPa, indicating that the introduction of human dECM significantly lowered the elastic modulus. A similar trend was measured for both soft and stiffened conditions. Conversely, the equilibrium swelling ratio of hybrid-hydrogels was significantly higher than that of synthetic hydrogels, indicating that incorporation of human dECM led to higher water absorption in the hydrogel (Figure 3B). The volumetric swelling ratio increased from 2.07 ± 0.15 for fully synthetic hydrogels to 18.81 ± 0.83 for hybrid-hydrogels containing 10% dECM. This phenomenon could be due to the strong hydrogen bonding between protein fragments in dECM and water molecules, which led to higher water molecule retention in the hydrogel network. Moreover, the swelling capacity of soft hybrid-hydrogels was twice that of the stiffened, indicating that free-radical homopolymerization did increase the crosslinking density of the network. A similar pattern of increased swelling and decreased modulus was observed by Yang et al. when increasing the azide-functionalized RGD peptide concentration in PEG-peptide hybrid-

https://doi.org/10.1021/acsami.2c18330
ACS Appl. Mater. Interfaces XXXX, XXX, XXX−XXX

hydrogels.[48] Rizzi, et al. have shown that the elastic moduli and swelling ratios of the protein-*co*-PEG hydrogels could be varied as a function of the stoichiometry of the reactive groups and precursor concentration.[49] These hybrid-hydrogel networks exhibited higher values for elastic modulus and lower values for swelling ratio when the thiol content on precursor proteins increased. In this study, the same thiol concentration was maintained for each concentration of human dECM. Hence, hybrid-hydrogels with high dECM content showed lower elastic modulus and higher swelling capacity. The same trend of swelling degree and crosslinking density was observed in photoinitiated methacrylated-hyaluronic acid hydrogel networks where high macromer concentration in networks exhibited lower swelling ratios and higher crosslinking densities.[50] The changes in the swelling ratio were characterized as a function of degradation time in degradable synthetic hydrogel networks; furthermore, swelling ratios and degradation rates were compared to changing chemistries between copolymerizing macromers.[51] These studies reinforced that the chemistry and functionality of hydrogel networks directly influence hydrogel mechanical properties.

The number-average molecular weight between crosslinks (M_c) was calculated to confirm this observation. M_c and mesh size followed the same trend as the swelling ratio, indicating that the incorporation of human dECM increased the distance between the network junctions. The M_c was calculated to be 0.11 ± 0.01 kg mol^{-1} for the soft synthetic hydrogel and 3.77 ± 0.18 kg mol^{-1} for the soft hybrid-hydrogel with 10% human dECM. This significant increase in M_c was due to both the higher molecular weight of the dECM crosslinker, which exhibited protein fragments up to 250 kDa compared to DTT (154.23 g mol^{-1}) and may also have been influenced by the unfolding of the coiled structure of human dECM. Previous studies of PEG-peptide hydrogels used circular dichroism spectrometry to demonstrate that coiled peptide structures influenced entanglements and resulted in a higher degree of swelling.[48] In natural hydrogels, collagen chains were observed to form new hydrogen bonds with water as well as within the collagen chain itself, thereby increasing the swelling ratio of collagen-based hydrogels.[52] Similarly, the coiled structure of human dECM used in this hybrid-hydrogel could lead to entanglements and increase hydrogen bonding between water molecules and hydrogel network. This reasoning would predict that, compared to synthetic hydrogels, hybrid-hydrogels should display a higher level of swelling, higher M_c, and higher mesh size, as measured here. These results were also in agreement with a study that observed increased swelling capacity of poly(acrylic acid) hydrogels with the incorporation of up to 6.7 wt % pectin. Interestingly, increasing the amount of pectin beyond 6.7 wt % led to a decrease in swelling, illustrating that beyond a point, higher crosslinking density will inevitably lead to lower mesh size in the network, reducing the swelling capacity.[53] These results have implications for future hybrid-hydrogel designs using dECM. In this study, incorporation of up to 10% dECM resulted in increased swelling ratios that appeared to be reaching a plateau (Figure 3B). Increasing the amount of dECM beyond 10% in hybrid-hydrogel formulations may lead to decreases in the swelling ratio. At the ratios studied here, the incorporation of dECM into hybrid-hydrogels appeared to increase hydrogen bond formation within the peptide fragments, contributing to increased swelling and higher mesh size in the network.

The mesh size of the soft synthetic hydrogel was calculated to be 1.07 ± 0.20 nm compared to 10.37 ± 0.63 nm for the soft hybrid-hydrogel consisting of 10% human dECM, indicating that the mesh size of the network was significantly increased with the incorporation of human dECM. Since the overall mesh size was higher in hybrid-hydrogels than in fully synthetic hydrogels, these biomaterials could be more permissive to the diffusion of bioactive molecules and migration of cells through the complex network structure, making the use of these hybrid-hydrogels within three-dimensional (3D) models even more physiologically relevant. Also, lower estimated mesh size and M_c for the stiffened conditions compared to soft hydrogels were observed again showing crosslink density increased after the photoinitiated homopolymerization of excess αMA moieties.

The theoretical and measured shear moduli of synthetic hydrogels and hybrid-hydrogels containing 10% dECM and synthetic hydrogel containing 100% DTT as the crosslinker were compared to better understand changes in network structure and mechanical properties that occurred when adding dECM into the PEG-based system (Table 1). Synthetic

Table 1. Comparison of Theoretical and Measured Shear Moduli (G) of Synthetic and Hybrid-Hydrogels

	theoretical G^a (kPa)	measured G (kPa)
synthetic (soft)	4.70 ± 0.2	1.31 ± 0.01
hybrid (soft)	3.26 ± 0.1	1.6 ± 0.09
synthetic (stiffened)	5.98 ± 0.5	4.17 ± 0.10
hybrid (stiffened)	5.02 ± 0.6	4.64 ± 0.14

[a]Theoretical G was calculated by rubberlike elasticity theory using eq 5.

hydrogel theoretical shear moduli were measured to be 4.7 ± 0.2 and 5.98 ± 0.5 kPa for soft and stiffened conditions, respectively, whereas measured shear moduli for synthetic hydrogels were 1.31± 0.01 and 4.17 ± 0.1 kPa, for soft and stiffened conditions, respectively, giving a greater difference between theoretical and measured shear moduli for synthetic hydrogels than for hybrid-hydrogels in both soft and stiffened conditions. These differences between theoretical and measured shear modulus may be attributed to nonideal crosslinking behavior.[54,55] Poor accessibility of crosslinking sites during gelation, due to steric hindrance or crosslinker molecular weight, could have led to the presence of dangling chains within the polymer network where one end is attached at a crosslinking point and the other end is not attached to the network and thus elastically inactive.[49] Synthetic hydrogels contain only DTT, a short crosslinker (154 g mol^{-1}), which could have led to dangling chains because it was not long enough to react with two other molecules. An increased number of dangling chains lowers the overall crosslinking density, thereby reducing elastic recovery and increasing swelling ratio. For example, in 4-arm star PEG (25 kDa) hydrogels, when the concentration was too low or too high, a short crosslinker could not link the star polymer efficiently. The resultant hydrogel network contained defects such as dangling chains or loops and showed heterogeneity in the viscoelastic measurements.[56]

Incorporating human dECM into the PEG hydrogels potentially decreased the number of dangling chains because

https://doi.org/10.1021/acsami.2c18330
ACS Appl. Mater. Interfaces XXXX, XXX, XXX−XXX

human dECM was significantly higher in molecular weight (130−250 kDa) than the synthetic crosslinker (DTT; MW = 154 g mol^{-1}). Even though a greater extent of dangling chains has been observed to result in a higher swelling ratio,[57] synthetic hydrogels displayed reduced swelling compared to hybrid-hydrogels. This outcome may result from hydrogen-bonding interactions between dECM and water molecules at equilibrium, which more strongly contribute to increases in swelling than dangling chains in the synthetic hydrogel. Similarly, Kyburz and Anseth illustrated that a network with a high degree of physical entanglements can display a greater measured modulus than the theoretical modulus.[58] A reduced difference between theoretical and measured shear moduli for hybrid-hydrogels may be attributed to the physical entanglements of the human dECM in the hydrogel. Additionally, minor differences in pH during a Michael addition reaction could have resulted in slightly different reaction kinetics or yields contributing to the differences between theoretical and measured modulus values.[59]

Many strategies have emerged recently to functionalize biomacromolecules for incorporation into biomaterials that present tissue-specific cues.[60] Here, chemically functionalized human dECM was successfully incorporated into hybrid-hydrogels to recapitulate human healthy and fibrotic tissues. The incorporation of human dECM into hybrid-hydrogels not only provided a physiological biochemical component to the biomaterials, but also significantly influenced network properties such as swelling, average molecular weight between crosslinks, and mesh size.

Cell Activation. Myofibroblasts are critical mediators of fibrotic progression. Previous studies have shown that composition and increases in microenvironmental stiffness can promote the activation of fibroblasts to myofibroblasts, as demonstrated by both the expression of αSMA stress fibers and enhanced cell spreading.[61,62] Booth et al. observed a significant increase in αSMA expression on acellular fibrotic human lung tissue compared to normal human lung tissue and demonstrated that fibrotic dECM was sufficient to induce fibroblast activation.[39] Due to the simultaneous biochemical and mechanical changes that occur during fibrosis, it was not possible in that study to determine which factor was the more potent driver of fibroblast activation. Studies of cellular responses to increased microenvironmental modulus have therefore relied on hydrogels with tunable mechanical properties. For example, a pronounced increase in αSMA expression in cardiac fibroblasts was observed on stiffer hyaluronic acid hydrogels (50 kPa) compared to cells cultured on 8 kPa hyaluronic acid hydrogels that recapitulate healthy myocardium.[63] However, recent studies using models designed to decouple fibrotic composition from mechanical stress showed that material stiffness is the dominant factor that affects the activation of fibroblasts.[23,64] In particular, Nizamoglu et al. created hydrogels from porcine dECM that could be stiffened using a ruthenium and sodium persulfate-initiated reaction to crosslink tyrosine moieties on the dECM. Results of fibroblast activation studies using this model showed increased activation induced by stiffening, even when the dECM composition of the hydrogel remained the same.[14] Similarly, murine fibroblasts cultured on PEG-based hybrid-hydrogels consisting of porcine dECM[22] and murine dECM[23] showed prominent Col1a1 and αSMA expression on stiffened hydrogels. When dECM derived from fibrotic murine lung was incorporated into hybrid-hydrogels, it only induced modest changes to fibroblast activation relative to the robust changes induced by stiffness.[23]

In this study, human fibroblasts were seeded on two-dimensional (2D) soft hybrid-hydrogels and then exposed to dynamic stiffening *via* dual-stage polymerization. Fibroblast activation was measured by assessing cell morphology based on f-actin expression and myofibroblast phenotype by αSMA expression, the combination of which correlates to high expression of a fibroblast activation genetic program.[32] Immunofluorescence staining for f-actin revealed a significant increase in cellular aspect ratio—the ratio between the major and minor axes of an ellipse fit to the cell area. Increasing aspect ratio indicates increased cellular elongation. On soft hybrid-hydrogels, fibroblasts remained rounded, while fibroblasts on stiffened hybrid-hydrogels began to stretch out protrusions that increased the average aspect ratio from 1.59 ± 0.02 to 2.98 ± 0.20 (Figure 4C). Similarly, stiffening resulted in a greater proportion of activated (noncircular, αSMA+) fibroblasts[32] from 25.8% on soft hybrid-hydrogels to 49.1% on stiffened samples (Figure 4D).

These results demonstrated the ability of this fully human hybrid-hydrogel culture model to facilitate investigation of dynamic fibroblast mechanosensing, a critical component of fibrotic progression. The experiments reported here were performed with a fixed concentration of dECM in the hybrid-hydrogel formulation. Future experiments could investigate how cell behavior changes in response to increased or decreased dECM content, which would alter the availability of cellular binding sites and signaling moieties in conjunction with the changes dECM brings to the material properties of the hybrid-hydrogel. This hybrid-hydrogel system could also support encapsulation of cells in 3D to investigate cellular responses to dynamic stiffening in an environment that is both biochemically relevant and mechanically tunable. Viability results for fibroblasts encapsulated within the 10 mol % dECM hybrid-hydrogels in 3D showed 49 ± 13% of the cells imaged were alive one day after encapsulation and this level of viability was maintained (43 ± 8%) over the next 3 days (Figure S6). These results indicate it is feasible to use hybrid-hydrogels for 3D investigations of cell−matrix interactions in fibrosis; however, it will be important to optimize the initial encapsulation conditions to improve initial cellular viability. One way to improve initial viability might be to use catalytic amine buffers that have been shown to have low cytotoxicity to initial the Michael addition reaction.[65]

CONCLUSIONS

A dynamically tunable hybrid-hydrogel system containing chemically modified human dECM was engineered to study fibroblast−matrix interactions *in vitro*. By incorporating intact, tissue-derived dECM, key biochemical properties of human tissue were recapitulated while taking advantage of dual-stage photopolymerization techniques to mimic the dynamic increase in microenvironmental stiffness observed during fibrotic progression in human organs. The incorporation of dECM altered key network properties of the hydrogels, including increasing the swelling ratio, average molecular weight between crosslinks, and mesh size, while decreasing the average shear modulus of the resulting hybrid-hydrogels. Focusing on the lung as a model system, fibroblast activation was measured in response to stiffening on human hybrid-hydrogels and was shown to increase with increasing elastic modulus. Hybrid-hydrogels could also be generated with

https://doi.org/10.1021/acsami.2c18330
ACS Appl. Mater. Interfaces XXXX, XXX, XXX−XXX

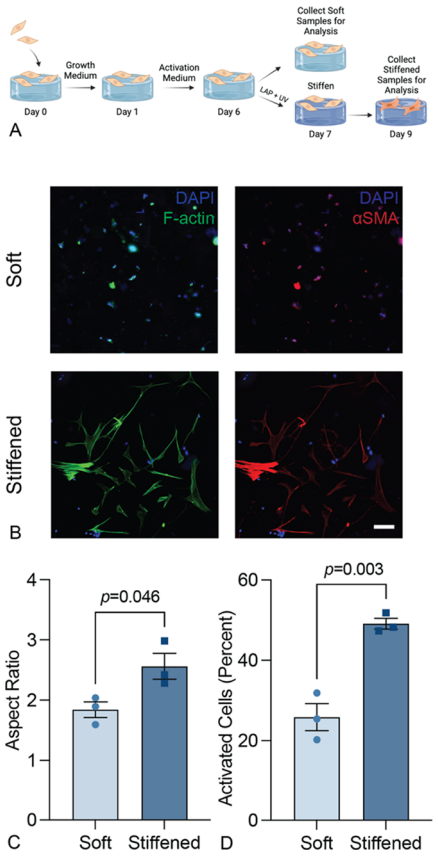

Figure 4. (A) Schematic diagram of the timeline for cell activation experiments. HPFs were cultured on soft hydrogels on day 0. Cells were cultured in 1% FBS media for all conditions. The photoinitiator (LAP) was added to culture media on day 6 for hydrogels to be stiffened and 365 nm UV light at mW cm^{-2} was applied for 5 min on day 7. Samples were collected and analyzed on day 7 and day 9 for soft and stiffened, respectively. Figure created with BioRender.com. (B) Representative images of human pulmonary fibroblasts on soft and stiffened hybrid-hydrogels showed expression of f-actin (green) and αSMA (red) with the DAPI staining (blue). On stiffened conditions, fibroblasts demonstrated increased spreading and increased actin organization compared to fibroblasts cultured on soft hybrid-hydrogels. (C) Quantification of average cellular aspect ratio showed higher levels of cell spreading on stiffened hybrid-hydrogels compared to soft hybrid-hydrogels ($p < 0.046$, $n = 3$). Each dot represents one experiment with $n = 3–6$ technical replicates. (D) Quantification of the percentage of fibroblasts displaying an activated (spread and αSMA^{+}) phenotype[32] showed a higher percentage of activated fibroblasts on stiffened hybrid-hydrogels compared to soft controls ($p = 0.003$, $n = 3$). Each dot represents one experiment with $n = 3–6$ technical replicates.

dECM sourced from specific tissues to provide the most physiologically relevant environment for a variety of cell types, improving the study of cellular and molecular mechanisms underlying fibrotic disease initiation and progression.

■ ASSOCIATED CONTENT

Data Availability Statement

The raw and processed data required to reproduce these findings are available here: Hewawasam, Rukshika; Šerbedžija, Predrag; Blomberg, Rachel; Magin, Chelsea (2022), "Chemical modification of human decellularized extracellular matrix for incorporation into phototunable hybrid-hydrogel models of tissue fibrosis", Mendeley Data, V3, doi: 10.17632/j3vbb6yfdv.1

Supporting Information

The Supporting Information is available free of charge at https://pubs.acs.org/doi/10.1021/acsami.2c18330.

PEGαMA NMR spectrum (Figure S1); total protein concentration measured by absorbance (Figure S2); thiol concentration versus TCEP molar excess (Figure S3); human growth factor array methods; human growth factor array (Table S1); human growth factor array results (Figure S4); Alcian blue staining of hybrid-hydrogels for GAGs (Figure S5); Picrosirius red staining and quantification of hybrid-hydrogels for collagen (Figure S6); and 3D Viability Methods; 3D fibroblast viability results (Figure S7) (PDF)

■ AUTHOR INFORMATION

Corresponding Author

Chelsea M. Magin − *Department of Bioengineering, University of Colorado, Aurora, Colorado 80045-2559, United States; Department of Pediatrics and Division of Pulmonary Sciences and Critical Care Medicine, Department of Medicine, University of Colorado, Aurora, Colorado 80045-2559, United States;* orcid.org/0000-0002-6988-8584; Email: chelsea.magin@cuanschutz.edu

Authors

Rukshika S. Hewawasam − *Department of Bioengineering, University of Colorado, Aurora, Colorado 80045-2559, United States*

Rachel Blomberg − *Department of Bioengineering, University of Colorado, Aurora, Colorado 80045-2559, United States*

Predrag Šerbedžija − *Department of Bioengineering, University of Colorado, Aurora, Colorado 80045-2559, United States*

Complete contact information is available at: https://pubs.acs.org/10.1021/acsami.2c18330

Author Contributions

R.S.H., P.S., R.B., and C.M.M. conceived the research plan. R.S.H., P.S., and R.B. carried out the experiments. All authors wrote, reviewed, and edited the manuscript.

Notes

The authors declare the following competing financial interest(s): C.M.M. and R.S.H. are inventors on a pending patent related to this technology. P.S. and R.B. declare no competing financial interest.

■ ACKNOWLEDGMENTS

This work was supported by funding from the National Heart, Lung, and Blood Institute of the National Institutes of Health (NIH) under awards R01 HL153096 (C.M.M., P.S., and R.B.) and T32 HL 07085 (R.B.); the National Cancer Institute of the NIH under award R21 CA252172 (C.M.M. and R.B.); the National Science Foundation under award 1941401 (C.M.M. and R.H.); and the Department of the Army under award W81XWH-20-1-0037 (C.M.M.).

■ REFERENCES

(1) Ben Amar, M.; Bianca, C. Towards a Unified Approach in the Modeling of Fibrosis: A review with research perspectives. *Phys. Life Rev.* **2016**, *17*, 61–85.

(2) Parker, M. W.; Rossi, D.; Peterson, M.; Smith, K.; Sikström, K.; White, E. S.; Connett, J. E.; Henke, C. A.; Larsson, O.; Bitterman, P. B. Fibrotic Extracellular Matrix Activates a Profibrotic Positive Feedback Loop. *J. Clin. Invest.* **2014**, *124*, 1622−1635.
(3) Herrera, J.; Henke, C. A.; Bitterman, P. B. Extracellular Matrix as a Driver of Progressive Fibrosis. *J. Clin. Invest.* **2018**, *128*, 45−53.
(4) Vijayaraj, P.; Minasyan, A.; Durra, A.; Karumbayaram, S.; Mehrabi, M.; Aros, C. J.; Ahadome, S. D.; Shia, D. W.; Chung, K.; Sandlin, J. M.; et al. Modeling Progressive Fibrosis with Pluripotent Stem Cells Identifies an Anti-fibrotic Small Molecule. *Cell Rep.* **2019**, *29*, 3488−3505.e3489.
(5) Bailey, K. E.; Floren, M. L.; D'Ovidio, T. J.; Lammers, S. R.; Stenmark, K. R.; Magin, C. M. Tissue-Informed Engineering Strategies for Modeling Human Pulmonary Diseases. *Am. J. Physiol.: Lung Cell. Mol. Physiol.* **2019**, *316*, L303−L320.
(6) Bucchieri, F.; Pitruzzella, A.; Fucarino, A.; Gammazza, A. M.; Bavisotto, C. C.; Marciano, V.; Cajozzo, M.; Lo Iacono, G.; Marchese, R.; Zummo, G.; et al. Functional Characterization of a Novel 3D Model of the Epithelial-Mesenchymal Trophic Unit. *Exp. Lung Res.* **2017**, *43*, 82−92.
(7) Strikoudis, A.; Cieslak, A.; Loffredo, L.; Chen, Y. W.; Patel, N.; Saqi, A.; Lederer, D. J.; Snoeck, H. W. Modeling of Fibrotic Lung Disease Using 3D Organoids Derived from Human Pluripotent Stem Cells. *Cell Rep.* **2019**, *27*, 3709−3723.e5.
(8) Tan, Q.; Ma, X. Y.; Liu, W.; Meridew, J. A.; Jones, D. L.; Haak, A. J.; Sicard, D.; Ligresti, G.; Tschumperlin, D. J. Nascent Lung Organoids Reveal Epithelium- and Bone Morphogenetic Protein-mediated Suppression of Fibroblast Activation. *Am. J. Respir. Cell Mol. Biol.* **2019**, *61*, 607−619.
(9) Bersini, S.; Gilardi, M.; Ugolini, G. S.; Sansoni, V.; Talo, G.; Perego, S.; Zanotti, S.; Ostano, P.; Mora, M.; Soncini, M.; et al. Engineering an Environment for the Study of Fibrosis: A 3D Human Muscle Model with Endothelium Specificity and Endomysium. *Cell Rep.* **2018**, *25*, 3858−3868 e3854.
(10) de Giorgio-Miller, A.; Bottoms, S.; Laurent, G.; Carmeliet, P.; Herrick, S. Fibrin-Induced Skin Fibrosis in Mice Deficient in Tissue Plasminogen Activator. *Am. J. Pathol.* **2005**, *167*, 721−732.
(11) Sundarakrishnan, A.; Zukas, H.; Coburn, J.; Bertini, B. T.; Liu, Z.; Georgakoudi, I.; Baugh, L.; Dasgupta, Q.; Black, L. D.; Kaplan, D. L. Bioengineered in Vitro Tissue Model of Fibroblast Activation for Modeling Pulmonary Fibrosis. *ACS Biomater. Sci. Eng.* **2019**, *5*, 2417−2429.
(12) Liu, L.; You, Z.; Yu, H.; Zhou, L.; Zhao, H.; Yan, X.; Li, D.; Wang, B.; Zhu, L.; Xu, Y.; et al. Mechanotransduction-Modulated Fibrotic Microniches Reveal the Contribution of Angiogenesis in Liver Fibrosis. *Nat. Mater.* **2017**, *16*, 1252−1261.
(13) Dunphy, S. E.; Bratt, J. A.; Akram, K. M.; Forsyth, N. R.; El Haj, A. J. Hydrogels for Lung Tissue Engineering: Biomechanical Properties of Thin Collagen-Elastin Constructs. *J. Mech. Behav. Biomed. Mater.* **2014**, *38*, 251−259.
(14) Nizamoglu, M.; de Hilster, R. H. J.; Zhao, F.; Sharma, P. K.; Borghuis, T.; Harmsen, M. C.; Burgess, J. K. An In Vitro Model of Fibrosis using Crosslinked Native Extracellular Matrix-Derived Hydrogels to Modulate Biomechanics Without Changing Composition. *Acta Biomater.* **2022**, *147*, 50−62. From NLM Medline
(15) Ravichandran, A.; Murekatete, B.; Moedder, D.; Meinert, C.; Bray, L. J. Photocrosslinkable Liver Extracellular Matrix Hydrogels for the Generation of 3D Liver Microenvironment Models. *Sci. Rep.* **2021**, *11*, No. 15566.
(16) Sakina, R.; Llucia-Valldeperas, A.; Henriques Lourenco, A.; Harichandan, A.; Gelsomino, S.; Wieringa, P.; Mota, C.; Moroni, L. Decellularization of Porcine Heart Tissue to Obtain Extracellular Matrix Based Hydrogels. *Methods Cell Biol.* **2020**, *157*, 3−21. From NLM Medline
(17) Porras, A. M.; Hutson, H. N.; Berger, A. J.; Masters, K. S. Engineering Approaches to Study Fibrosis in 3-D In Vitro Systems. *Curr. Opin. Biotechnol.* **2016**, *40*, 24−30.
(18) Nair, L. S.; Laurencin, C. T. Biodegradable Polymers as Biomaterials. *Prog. Polym. Sci.* **2007**, *32*, 762−798.
(19) de Hilster, R. H. J.; Sharma, P. K.; Jonker, M. R.; White, E. S.; Gercama, E. A.; Roobeek, M.; Timens, W.; Harmsen, M. C.; Hylkema, M. N.; Burgess, J. K. Human Lung Extracellular Matrix Hydrogels Resemble the Stiffness and Viscoelasticity of Native Lung Tissue. *Am. J. Physiol.: Lung Cell. Mol. Physiol.* **2020**, *318*, L698−L704.
(20) Hjortnaes, J.; Camci-Unal, G.; Hutcheson, J. D.; Jung, S. M.; Schoen, F. J.; Kluin, J.; Aikawa, E.; Khademhosseini, A. Directing Valvular Interstitial Cell Myofibroblast-Like Differentiation in a Hybrid Hydrogel Platform. *Adv. Healthcare Mater.* **2015**, *4*, 121−130.
(21) Duan, B.; Hockaday, L. A.; Kapetanovic, E.; Kang, K. H.; Butcher, J. T. Stiffness and Adhesivity Control Aortic Valve Interstitial Cell Behavior Within Hyaluronic Acid Based Hydrogels. *Acta Biomater.* **2013**, *9*, 7640−7650.
(22) Petrou, C. L.; D'Ovidio, T. J.; Bolukbas, D. A.; Tas, S.; Brown, R. D.; Allawzi, A.; Lindstedt, S.; Nozik-Grayck, E.; Stenmark, K. R.; Wagner, D. E.; Magin, C. M. Clickable Decellularized Extracellular Matrix as a New Tool for Building Hybrid-Hydrogels to Model Chronic Fibrotic Diseases In Vitro. *J. Mater. Chem. B* **2020**, *8*, 6814−6826.
(23) Saleh, K. S.; Hewawasam, R.; Serbed, P.; Blomberg, R.; Noreldeen, S. E.; Edelman, B.; Smith, B. J.; Riches, D. W. H.; Magin, C. M. Engineering Hybrid-Hydrogels Comprised of Healthy or Diseased Decellularized Extracellular Matrix to Study Pulmonary Fibrosis. *Cell Mol. Bioeng.* **2022**, *15*, 505−519.
(24) Meyvis, T. K. L.; De Smedt, S. C.; Demeester, J.; Hennink, W. E. Rheological Monitoring of Long-Term Degrading Polymer Hydrogels. *J. Rheol.* **1999**, *43*, 933−950.
(25) Richbourg, N. R.; Wancura, M.; Gilchrist, A. E.; Toubbeh, S.; Harley, B. A. C.; Cosgriff-Hernandez, E.; Peppas, N. A. Precise Control of Synthetic Hydrogel Network Structure via Linear, Independent Synthesis-Swelling Relationships. *Sci. Adv.* **2021**, *7*, No. eabe3245.
(26) Richbourg, N. R.; Peppas, N. A. The Swollen Polymer Network Hypothesis: Quantitative Models of Hydrogel Swelling, Stiffness, and Solute Transport. *Prog. Polym. Sci.* **2020**, *105*, No. 101243.
(27) Merrill, E. W.; Dennison, K. A.; Sung, C. Partitioning and Diffusion of Solutes in Hydrogels of Poly(ethylene oxide). *Biomaterials* **1993**, *14*, 1117−1126.
(28) Yang, T.; Long, H.; Malkoch, M.; Gamstedt, E. K.; Berglund, L.; Hult, A. Characterization of Well-Defined Poly(ethylene glycol) Hydrogels Prepared by Thiol-ene Chemistry. *J. Polym. Sci., Part A: Polym. Chem.* **2011**, *49*, 4044−4054.
(29) Rehmann, M. S.; Skeens, K. M.; Kharkar, P. M.; Ford, E. M.; Maverakis, E.; Lee, K. H.; Kloxin, A. M. Tuning and Predicting Mesh Size and Protein Release from Step Growth Hydrogels. *Biomacromolecules* **2017**, *18*, 3131−3142.
(30) Lutolf, M. P.; Hubbell, J. A. Synthesis and Physicochemical Characterization of End-Linked Poly(ethylene glycol)-co-peptide Hydrogels Formed by Michael-Type Addition. *Biomacromolecules* **2003**, *4*, 713−722.
(31) Magin, C. M.; Anseth, K. S. In Situ Control of Cell Substrate Microtopographies Using Photolabile Hydrogels. *Small* **2013**, *9*, 578−584.
(32) Hillsley, A.; Santoso, M. S.; Engels, S. M.; Halwachs, K. N.; Contreras, L. M.; Rosales, A. M. A Strategy to Quantify Myofibroblast Activation on a Continuous Spectrum. *Sci. Rep.* **2022**, *12*, No. 12239.
(33) Wolters, P. J.; Collard, H. R.; Jones, K. D. Pathogenesis of Idiopathic Pulmonary Fibrosis. *Annu. Rev. Pathol.: Mech. Dis.* **2014**, *9*, 157−179.
(34) Dooling, L. J.; Saini, K.; Anlas, A. A.; Discher, D. E. Tissue Mechanics Coevolves with Fibrillar Matrisomes in Healthy and Fibrotic Tissues. *Matrix Biol.* **2022**, *111*, 153−188.
(35) Mueller, S.; Sandrin, L. Liver Stiffness: a Novel Parameter for the Diagnosis of Liver Disease. *Hepatic Med.: Evidence Res.* **2010**, *2*, 49−67.
(36) Rojkind, M.; Giambrone, M. A.; Biempica, L. Collagen Types in Normal and Cirrhotic Liver. *Gastroenterology* **1979**, *76*, 710−719.
(37) Chen, W.; Rock, J. B.; Yearsley, M. M.; Ferrell, L. D.; Frankel, W. L. Different Collagen Types Show Distinct Rates of Increase From

https://doi.org/10.1021/acsami.2c18330
ACS Appl. Mater. Interfaces XXXX, XXX, XXX−XXX

Early to Late Stages of Hepatitis C-Related Liver Fibrosis. *Hum. Pathol.* **2014**, *45*, 160−165.
(38) van Putten, S.; Shafieyan, Y.; Hinz, B. Mechanical Control of Cardiac Myofibroblasts. *J. Mol. Cell. Cardiol.* **2016**, *93*, 133−142.
(39) Booth, A. J.; Hadley, R.; Cornett, A. M.; Dreffs, A. A.; Matthes, S. A.; Tsui, J. L.; Weiss, K.; Horowitz, J. C.; Fiore, V. F.; Barker, T. H.; et al. Acellular Normal and Fibrotic Human Lung Matrices as a Culture System for In Vitro Investigation. *Am. J. Respir. Crit. Care Med.* **2012**, *186*, 866−876.
(40) Tian, Y. Q.; Li, H.; Gao, Y. J.; Liu, C. M.; Qiu, T.; Wu, H. Y.; Cao, M. S.; Zhang, Y. W.; Ding, H.; Chen, J. Y.; Cai, H. Quantitative Proteomic Characterization of Lung Tissue in Idiopathic Pulmonary Fibrosis. *Clin. Proteom.* **2019**, *16*, No. 6.
(41) Åhrman, E.; Hallgren, O.; Malmstrom, L.; Hedstrom, U.; Malmstrom, A.; Bjermer, L.; Zhou, X. H.; Westergren-Thorsson, G.; Malmstrom, J. Quantitative Proteomic Characterization of the Lung Extracellular Matrix in Chronic Obstructive Pulmonary Disease and Idiopathic Pulmonary Fibrosis. *J. Proteomics* **2018**, *189*, 23−33.
(42) de Hilster, R. H.; Jonker, M. R.; Sharma, P. K.; Hylkema, M. N.; Harmsen, M. C.; Burgess, J. K. Human Lung Extracellular Matrix Hydrogels Replicate Biomechanics of Diseased and Nondiseased Lung. *Am. J. Respir. Crit. Care Med.* **2019**, *199*, A2555.
(43) Uhl, F. E.; Zhang, F.; Pouliot, R. A.; Uriarte, J. J.; Rolandsson Enes, S.; Han, X.; Ouyang, Y.; Xia, K.; Westergren-Thorsson, G.; Malmström, A.; et al. Functional Role of Glycosaminoglycans in Decellularized Lung Extracellular Matrix. *Acta Biomater.* **2020**, *102*, 231−246. From NLM
(44) Lattouf, R.; Younes, R.; Lutomski, D.; Naaman, N.; Godeau, G.; Senni, K.; Changotade, S.; et al. Picrosirius Red Staining: A Useful Tool to Appraise Collagen Networks in Normal and Pathological Tissues. *J. Histochem. Cytochem.* **2014**, *62*, 751−758.
(45) Kloxin, A. M.; Benton, J. A.; Anseth, K. S. In Situ Elasticity Modulation with Dynamic Substrates to Direct Cell Phenotype. *Biomaterials* **2010**, *31*, 1−8.
(46) Islamoglu, M. S.; Gulcicek, S.; Seyahi, N. Kidney Tissue Elastography and Interstitial Fibrosis Observed in Kidney Biopsy. *Renal Failure* **2022**, *44*, 314−319.
(47) Pouliot, R. A.; Link, P. A.; Mikhaiel, N. S.; Schneck, M. B.; Valentine, M. S.; Gninzeko, F. J. K.; Herbert, J. A.; Sakagami, M.; Heise, R. L. Development and Characterization of a Naturally Derived Lung Extracellular Matrix Hydrogel. *J. Biomed. Mater. Res., Part A* **2016**, *104*, 1922−1935.
(48) Liu, S. Q.; Ee, P. L.; Ke, C. Y.; Hedrick, J. L.; Yang, Y. Y. Biodegradable Poly(ethylene glycol)-Peptide Hydrogels with Well-Defined Structure and Properties for Cell Delivery. *Biomaterials* **2009**, *30*, 1453−1461.
(49) Rizzi, S. C.; Hubbell, J. A. Recombinant Protein-co-PEG Networks as Cell-Adhesive and Proteolytically Degradable Hydrogel Matrixes. Part 1: Development and physicochernical characteristics. *Biomacromolecules* **2005**, *6*, 1226−1238.
(50) Burdick, J. A.; Chung, C.; Jia, X. Q.; Randolph, M. A.; Langer, R. Controlled Degradation and Mechanical Behavior of Photopolymerized Hyaluronic Acid Networks. *Biomacromolecules* **2005**, *6*, 386−391.
(51) Martens, P. J.; Bryant, S. J.; Anseth, K. S. Tailoring the Degradation of Hydrogels Formed from Multivinyl Poly(ethylene glycol) and Poly(vinyl alcohol) Macromers for Cartilage Tissue Engineering. *Biomacromolecules* **2003**, *4*, 283−292.
(52) Tronci, G.; Grant, C. A.; Thomson, N. H.; Russell, S. J.; Wood, D. J. Multi-Scale Mechanical Characterization of Highly Swollen Photo-Activated Collagen Hydrogels. *J. R. Soc. Interface* **2015**, *12*, No. 20141079.
(53) Kowalski, G.; Kijowska, K.; Witczak, M.; Kuterasinski, L.; Lukasiewicz, M. Synthesis and Effect of Structure on Swelling Properties of Hydrogels Based on High Methylated Pectin and Acrylic Polymers. *Polymers* **2019**, *11*, No. 114.
(54) Winter, H. H.; Morganelli, P.; Chambon, F. Stoichiometry Effects on Rheology of Model Polyurethanes at the Gel Point. *Macromolecules* **1988**, *21*, 532−535.
(55) Chambon, F.; Winter, H. H. Linear Viscoelasticity at the Gel Point of a Cross-Linking Pdms with Imbalanced Stoichiometry. *J. Rheol.* **1987**, *31*, 683−697.
(56) Liu, W.; Gong, X. J.; Zhu, Y. W.; Wang, J. Q.; Ngai, T.; Wu, C. Probing Sol-Gel Matrices and Dynamics of Star PEG Hydrogels Near Overlap Concentration. *Macromolecules* **2019**, *52*, 8956−8966.
(57) Atta, A. M.; Abdel-Azim, A. A. A. Effect of Crosslinker Functionality on Swelling and Network Parameters of Copolymeric Hydrogels. *Polym. Adv. Technol.* **1998**, *9*, 340−348.
(58) Kyburz, K. A.; Anseth, K. S. Three-Dimensional hMSC Motility Within Peptide-Functionalized PEG-Based Hydrogels of Varying Adhesivity and Crosslinking Density. *Acta Biomater.* **2013**, *9*, 6381−6392.
(59) FitzSimons, T. M.; Anslyn, E. V.; Rosales, A. M. Effect of pH on the Properties of Hydrogels Cross-Linked via Dynamic Thia-Michael Addition Bonds. *ACS Polym. Au* **2022**, *2*, 129−136.
(60) Guo, J. L.; Kim, Y. S.; Mikos, A. G. Biomacromolecules for Tissue Engineering: Emerging Biomimetic Strategies. *Biomacromolecules* **2019**, *20*, 2904−2912.
(61) Shinde, A. V.; Humeres, C.; Frangogiannis, N. G. The Role of Alpha-Smooth Muscle Actin in Fibroblast-Mediated Matrix Contraction and Remodeling. *Biochim. Biophys. Acta, Mol. Basis Dis.* **2017**, *1863*, 298−309.
(62) Burgess, J. K.; Mauad, T.; Tjin, G.; Karlsson, J. C.; Westergren-Thorsson, G. The Extracellular Matrix - the Under-Recognized Element in Lung Disease? *J. Pathol.* **2016**, *240*, 397−409.
(63) Herum, K. M.; Choppe, J.; Kumar, A.; Engler, A. J.; McCulloch, A. D. Mechanical Regulation of Cardiac Fibroblast Profibrotic Phenotypes. *Mol. Biol. Cell* **2017**, *28*, 1871−1882.
(64) Sava, P.; Ramanathan, A.; Dobronyi, A.; Peng, X. Y.; Sun, H. X.; Ledesma-Mendoza, A.; Herzog, E. L.; Gonzalez, A. L. Human Pericytes Adopt Myofibroblast Properties in the Microenvironment of the IPF Lung. *JCI Insight* **2017**, *2*, No. e96352.
(65) Larsen, D.; Kietrys, A. M.; Clark, S. A.; Park, H. S.; Ekebergh, A.; Kool, E. T. Exceptionally Rapid Oxime and Hydrazone Formation Promoted by Catalytic Amine Buffers with Low Toxicity. *Chem. Sci.* **2018**, *9*, 5252−5259.

https://doi.org/10.1021/acsami.2c18330
ACS Appl. Mater. Interfaces XXXX, XXX, XXX−XXX